



Expanding Oxygen-Minimum Zones in the Tropical Oceans

Lothar Stramma, *et al.*
Science **320**, 655 (2008);
DOI: 10.1126/science.1153847

The following resources related to this article are available online at www.sciencemag.org (this information is current as of May 2, 2008):

Updated information and services, including high-resolution figures, can be found in the online version of this article at:

<http://www.sciencemag.org/cgi/content/full/320/5876/655>

This article **cites 13 articles**, 4 of which can be accessed for free:

<http://www.sciencemag.org/cgi/content/full/320/5876/655#otherarticles>

This article appears in the following **subject collections**:

Oceanography

<http://www.sciencemag.org/cgi/collection/oceans>

Information about obtaining **reprints** of this article or about obtaining **permission to reproduce this article** in whole or in part can be found at:

<http://www.sciencemag.org/about/permissions.dtl>

otic polyphosphate synthesis can only occur at the elevated temperatures characteristic of such extreme environments as hydrothermal vent systems (6). There is no evidence that the transformation of polyphosphate to apatite in marine sediments is dependent on the specific source of polyphosphate, however.

Enhanced phosphorus sequestration in marine sediments resulting from the conversion of diatom-derived polyphosphates to apatite may be manifested in the geologic record. The mid-Mesozoic rise of marine diatoms (28) coincides with a trend toward lower organic carbon to total phosphorus ratios in marine sediments (29). Because oceanic phosphorus influences atmospheric carbon dioxide levels over geologic time through regulation of marine primary productivity (2), geologic fluctuations in phosphorus burial efficiency brought on by changes in diatom abundance may have also exerted substantial paleoclimatic influences.

References and Notes

1. C. R. Benitez-Nelson, *Earth Sci. Rev.* **51**, 109 (2000).
2. P. Van Cappellen, E. D. Ingall, *Science* **271**, 493 (1996).
3. A. Paytan, K. McLaughlin, *Chem. Rev.* **107**, 563 (2007).
4. K. C. Ruttenger, R. A. Berner, *Geochim. Cosmochim. Acta* **57**, 991 (1993).

5. P. Van Cappellen, R. A. Berner, *Geochim. Cosmochim. Acta* **55**, 1219 (1991).
6. M. R. W. Brown, A. Kornberg, *Proc. Natl. Acad. Sci. U.S.A.* **101**, 16085 (2004).
7. P. Mateo, I. Douterelo, E. Berrendero, E. Perona, *J. Phycol.* **42**, 61 (2006).
8. K. M. Romans, E. J. Carpenter, *J. Phycol.* **30**, 935 (1994).
9. B. A. Lawrence *et al.*, *Microbiology* **169**, 195 (1998).
10. L. Solorzano, J. D. H. Strickland, *Limnol. Oceanogr.* **13**, 515 (1968).
11. K. Miyata, A. Hattori, A. Ohtsuki, *Mar. Biol.* **93**, 291 (1986).
12. M. J. Perry, *Limnol. Oceanogr.* **21**, 88 (1976).
13. D. M. Karl, K. M. Björkman, in *Biogeochemistry of Marine Dissolved Organic Matter*, D. A. Hansell, C. A. Carlson, Eds. (Academic Press, New York, 2002), chap. 6.
14. J. A. Brandes, E. Ingall, D. Paterson, *Mar. Chem.* **103**, 250 (2007).
15. T. A. Vetter, E. M. Perdue, E. Ingall, J.-F. Koprivnjak, P. H. Pfomrom, *Sep. Purif. Technol.* **56**, 383 (2007).
16. Materials and methods are available as supporting material on Science Online.
17. L. L. Clark, E. D. Ingall, R. Benner, *Am. J. Sci.* **299**, 724 (1999).
18. L. C. Kolowitz, E. D. Ingall, R. Benner, *Limnol. Oceanogr.* **46**, 309 (2001).
19. P. Sannigrahi, E. D. Ingall, R. Benner, *Geochim. Cosmochim. Acta* **70**, 5868 (2006).
20. K. O. Buesseler *et al.*, *Science* **316**, 567 (2007).
21. R. A. Armstrong, C. Lee, J. I. Hedges, S. Honjo, S. G. Wakeham, *Deep-Sea Res. II* **49**, 219 (2001).
22. K. Biddle, F. Azam, *Nature* **397**, 508 (1999).
23. X-ray fluorescence spectra and phosphorus elemental maps were collected at beamline 2-ID-B, Advanced Photon Source, Argonne National Laboratory.
24. P. Sannigrahi, E. Ingall, *Geochem. Trans.* **6**, 52 (2005).
25. L. L. Clark, E. D. Ingall, R. Benner, *Nature* **393**, 426 (1998).
26. H. N. Schulz, H. D. Schulz, *Science* **307**, 416 (2005).
27. F. Louanchi *et al.*, *Deep-Sea Res. I* **48**, 1581 (2001).
28. M. E. Katz, Z. V. Finkel, D. Grzebyk, A. H. Knoll, P. G. Falkowski, *Annu. Rev. Ecol. Syst.* **35**, 523 (2004).
29. T. J. Algeo, E. Ingall, *Palaeogeogr. Palaeoclimatol. Palaeoecol.* **256**, 130 (2007).
30. This material is based on work supported by NSF under grant 0526178. Use of the Advanced Photon Source is supported by the U.S. Department of Energy, Office of Basic Energy Sciences (DE-AC02-06CH11357). We thank the crew of the R/V Barnes; R. Keil and J. Nuwer for assistance with field sampling; S. Herron and G. Lyons for help during field sampling and sample analysis; R. Styles and C. Jackson for assistance with sample analysis; G. Patterson and J. Platenius of the Clayoquot Field Station in Tofino, British Columbia, for providing lab space and a welcoming base for our field studies; P. Sobczyk and members of her lab at Georgia Tech for the use of the epifluorescence microscope, and J. Leisen and L. Gelbaum for NMR assistance. The authors declare no competing financial interests.

Supporting Online Material

www.sciencemag.org/cgi/content/full/320/5876/652/DC1

Materials and Methods

SOM Text

Figs. S1 to S9

References and Notes

15 October 2007; accepted 24 March 2008

10.1126/science.1151751

Expanding Oxygen-Minimum Zones in the Tropical Oceans

Lothar Stramma,^{1*} Gregory C. Johnson,² Janet Sprintall,³ Volker Mohrholz⁴

Oxygen-poor waters occupy large volumes of the intermediate-depth eastern tropical oceans. Oxygen-poor conditions have far-reaching impacts on ecosystems because important mobile macroorganisms avoid or cannot survive in hypoxic zones. Climate models predict declines in oceanic dissolved oxygen produced by global warming. We constructed 50-year time series of dissolved-oxygen concentration for select tropical oceanic regions by augmenting a historical database with recent measurements. These time series reveal vertical expansion of the intermediate-depth low-oxygen zones in the eastern tropical Atlantic and the equatorial Pacific during the past 50 years. The oxygen decrease in the 300- to 700-m layer is 0.09 to 0.34 micromoles per kilogram per year. Reduced oxygen levels may have dramatic consequences for ecosystems and coastal economies.

Oceanic dissolved-oxygen concentrations affect marine biogeochemical processes and have major impacts on the global carbon and nitrogen cycles (1). These concentrations are very sensitive to changes in air-sea fluxes and interior ocean advection, hence dissolved oxygen is an important parameter for understanding the ocean's role in climate (2). Impor-

tant mobile macroorganisms are stressed or die under hypoxic conditions; that is, when oxygen concentrations drop below ~60 to 120 $\mu\text{mol kg}^{-1}$ (3). Hypoxia occurs at different oxygen concentrations among various species of macroorganisms, so the threshold is not precise. Regions with oxygen concentrations below about 10 $\mu\text{mol kg}^{-1}$ are termed suboxic. In suboxic regions, nitrate (if present) becomes involved in respiration (1). Anoxic regions have no dissolved oxygen. At present, the intermediate-depth low-oxygen layers, here called the oxygen-minimum zone (OMZ), are suboxic in the eastern tropical Pacific Ocean and the northern reaches of the tropical Indian Ocean and are hypoxic in the tropical Atlantic Ocean (Fig. 1).

Oceanic dissolved oxygen concentrations have varied widely in the geologic past. For instance,

paleoclimate records from the Cretaceous reveal profoundly altered biogeochemical cycles and dramatic consequences for ecosystems associated with reductions of ocean oxygen (4). The anoxic ocean at the end of the Permian (251 million years ago) is perhaps the most striking example, being associated with elevated atmospheric CO_2 and massive terrestrial and oceanic extinctions (5, 6).

Climate models predict an overall decline in oceanic dissolved oxygen concentration and a consequent expansion of the OMZ under global warming conditions (7), with the largest declines occurring in extratropical regions. In the tropical regions, the models predict either zonal mean oxygen increases at depths of about 200 to 1000 m in the Atlantic and Pacific Oceans (7) or moderate zonal mean oxygen decreases (8). Predicted oxygen changes in the thermocline waters result largely from solubility changes in the upstream source waters, whereas changes in the deeper waters result mainly from decreased interior advection and ongoing oxygen consumption by remineralization of sinking particulate organic matter (7).

The global ocean has warmed substantially over the past 50 years (9), and strong interannual-to-decadal variations of oxygen have been observed in the upper 100 m (10). Long-term oxygen changes have been observed and reported in the subpolar and subtropical regions (11, 12). For instance, in the subarctic Pacific at Ocean Station Papa (50°N, 145°W), declining oxygen concentrations have been reported from depths of 100 to 400 m between 1956 and 2006 (11). Ocean oxygen data from the most oxygen-poor tropical regions of the OMZ

¹Institut für Meereswissenschaften an der Universität Kiel (IFM-GEOMAR), Düsternbrooker Weg 20, 24105 Kiel, Germany.

²National Oceanic and Atmospheric Administration, Pacific Marine Environmental Laboratory, 7600 Sand Point Way NE, Seattle, WA 98115, USA. ³Scripps Institution of Oceanography, 9500 Gilman Drive, La Jolla, CA 92093, USA. ⁴Baltic Sea Research Institute Warnemünde, Post Office Box 301161, 18112 Rostock, Germany.

*To whom correspondence should be addressed. E-mail: lstramma@ifm-geomar.de

are limited, but some regions exist for which historical data can be augmented with data from recent survey programs to construct relatively long, quasi-continuous oxygen time series.

We constructed and analyzed oxygen time series in some select areas of the tropical oceans (Fig. 1), using quality-controlled historical data from the HydroBase 2 database (13) and more recently measured oxygen profiles. Only oxygen data collected since 1960 were used because older oxygen data are rare and the net effect of changes in the observation system on our ability to document real ocean variability is not well understood. Unfortunately, even after 1960 oxygen data in most tropical regions are too sparse to construct useful time series, because in the past most oxygen profiles were collected almost exclusively from ships dedicated to oceanographic research. Recently, a small fraction of the 3000 Argo freely drifting floats that report vertical profiles of temperature and salinity over the upper 2000 m of the ocean via satellite at 10-day intervals (14) have been equipped with oxygen sensors. These floats provide valuable oxygen profiles (15) that were used to expand our time series through 2007 in the tropical Atlantic.

Reductions in observed minimum oxygen concentrations and vertical expansion of the OMZ since 1960 are apparent in three areas of the tropical Atlantic Ocean (Fig. 2). In the oxygen-poor region of the tropical North Atlantic (Fig. 1; 10° to 14°N, 20° to 30°W), a time series of historical data was augmented with data from meridional hydrographic sections nominally along 29°W in July 2003 and 23°W in July 2006 (Fig. 2A). No seasonal signal is present in this area

(16). In the OMZ, core oxygen values decline and the OMZ expands vertically with time. The vertical extent of the layer with oxygen concentrations of $<90 \mu\text{mol kg}^{-1}$ increased 85%, from a thickness of 370 m in 1960 to 690 m in 2006. In the near-equatorial Atlantic Ocean, oxygen values are higher to both the north and south (Fig. 1) because of the eastward transport of relatively oxygen-rich water within the complicated tropical current system (17). The relatively oxygen-rich water in the Atlantic Central Water originates from the poleward side of the subtropical gyre. Historical data, hydrocasts from three repeat sections along 23°W since 2000, and two recent profiles from an Argo float allowed construction of a time series (Fig. 2B) in the central equatorial Atlantic (Fig. 1; 3°S to 3°N, 18° to 28°W). This time series also shows some indication of a reduced concentration at the vertical oxygen minimum over time and a vertical expansion of the oxygen-poor OMZ. Similarly, a tropical South Atlantic (Fig. 1; 14° to 8°S, 4° to 12°E) time series (Fig. 2C) also shows a vertical expansion of the OMZ; although there are long gaps after the late 1980s, and no data between 2001 and 2007, a recent preliminary calibrated oxygen profile taken at 9°S, 8°E in March 2008 is consistent with the trend of an oxygen decline.

The OMZ in the tropical North and South Pacific Oceans reaches suboxic (and, in the most oxygen-poor regions, nearly anoxic) levels (Fig. 1), so detecting changes in minimum values there is difficult. Furthermore, data in the most oxygen-poor regions are too sparse to allow the construction of quasi-continuous time

series. However, as in the Atlantic Ocean, Pacific equatorial currents carry relatively oxygen-rich water eastward toward the most oxygen-poor regions of the OMZ in both hemispheres. Historical hydrographic data in the eastern equatorial Pacific Ocean (Fig. 1; 5°S to 5°N, 105° to 115°W), augmented with data collected during some recent Tropical Atmosphere Ocean project mooring maintenance cruises along 110°W, constitute a time series (Fig. 2D) that reveals a vertical expansion of the OMZ. However, a depth-integrated oxygen trend there is not statistically significantly different from zero when a stringent 95% confidence criterion is used (Table 1). Slightly higher values from 1980 to 1990 may be caused by sample locations biased toward the equator, where more oxygen-rich waters are advected eastward from the west. In the central equatorial Pacific (Fig. 1; 5°S to 5°N, 165° to 175°W), oxygen concentrations within the OMZ are more variable (Fig. 2E). Nevertheless, the OMZ thickness expands over the duration of the time series. This vertical expansion with time is not closely related to a temperature increase; in both areas of the equatorial Pacific, the temperature in the 300- to 700-m layer slightly decreases, as does the oxygen content (Table 1).

In the Indian Ocean, the lowest oxygen values in the OMZ are not located in the eastern tropics as they are in the Atlantic and Pacific Oceans, but to the north in the Arabian Sea and the Bay of Bengal (Fig. 1). In addition, minimum oxygen concentrations within the Indian Ocean OMZ are generally deeper (near 800 m) than in the other two oceans. In the northern Indian Ocean OMZ, sources and sinks of oxygen are nearly in apparent balance; circulation there appears relatively stagnant, with detritus falling from the highly productive waters above and rapidly depleting oxygen below. As in the eastern tropical Pacific Ocean, oxygen values in the northern Indian Ocean OMZ are suboxic, and the sparse data distributions in the most oxygen-poor regions preclude the construction of long quasi-continuous time series there. However, the recent occupation of a meridional section nominally along 95°E made possible the construction of an eastern equatorial Indian Ocean time series (Fig. 1; 5°S to 0°, 90° to 98°E), despite gaps in data since the mid-1980s (Fig. 2F). Unlike the other time series presented here, there is neither an obvious increase of the vertical extent of the OMZ nor a visible decrease in oxygen minimum values. Statistics of the layer at a depth of 300 to 700 m reveal a weak oxygen decrease not different from zero at 95% confidence (Table 1). Time series from the early 1960s to the late 1990s (not shown) in the western equatorial Indian Ocean, the Arabian Sea, and the Bay of Bengal show similar constancy in the tropical Indian Ocean OMZ. Collectively, these results suggest that over the past few decades there has been no substantial change in the tropical Indian Ocean OMZ.

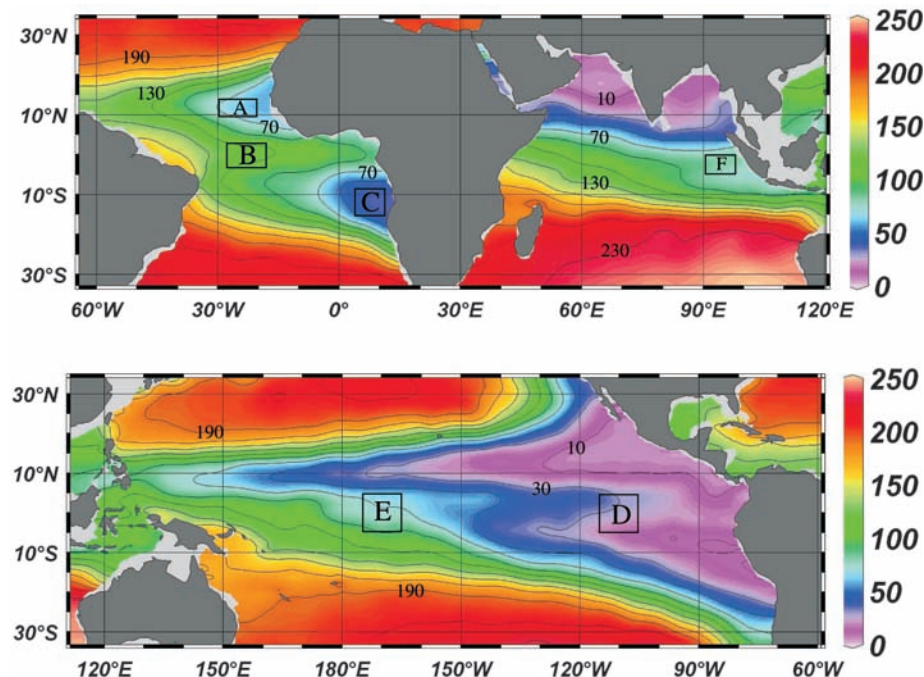


Fig. 1. Climatological mean (18) dissolved oxygen concentrations ($\mu\text{mol kg}^{-1}$ shown in color) at 400 m depth contoured at $20\text{-}\mu\text{mol kg}^{-1}$ intervals from 10 to $230 \mu\text{mol kg}^{-1}$ (black lines) using Ocean Data View (19) software. Analyzed areas (A to F, Table 1, and Fig. 2) are enclosed by black boxes.

As an auxiliary benefit, the constancy of OMZ characteristics in the Indian Ocean time series suggests that the changes observed in the tropical Atlantic and Pacific Ocean OMZ characteristics are not based on changes in observa-

tion techniques. This concern was also tested in the oxygen-rich deep-water formation region of the Labrador Sea, for which a very well-sampled time series can be constructed from 1960 to the present. There, no trend toward lower oxygen val-

ues is apparent, supporting the claim that oceanic oxygen measurements taken over the past 50 years are not subject to large observational biases that may produce spurious temporal trends.

The tropical ocean OMZs in the central and eastern tropical Atlantic and equatorial Pacific Oceans appear to have expanded and intensified during the past 50 years. Despite the sparseness of observations, the time series used show that the decline in oxygen content has been most intense in the tropical Atlantic, where at present hypoxic regions are small as compared with the Pacific and Indian Oceans. For these reasons, the Atlantic may also have the most potential for large increases in the area of hypoxic regions.

The observational analysis presented here supports climate model predictions of dissolved oxygen declines in the tropical ocean (7, 8) and an expansion of the tropical OMZs due to a contribution of thermal, dynamical, and biogeochemical factors (8). The observed oxygen declines reported here of 0.09 to 0.34 $\mu\text{mol kg}^{-1}\text{year}^{-1}$ for 300- to 700-m depths (Table 1) are somewhat smaller than those reported in the North Pacific (11) at 100 to 400 m. Together, these trends affect carbon and nitrogen cycles, with fundamental implications for marine ecosystems and thereby fisheries resource management issues. Given climate model projections, and the geological record that indicates times of widely distributed suboxic regions, sustained global ocean measurements of dissolved oxygen concentrations are needed (for instance, by equipping more Argo floats with well-calibrated dissolved oxygen sensors) to more closely monitor variations in the strength and extent of the OMZ.

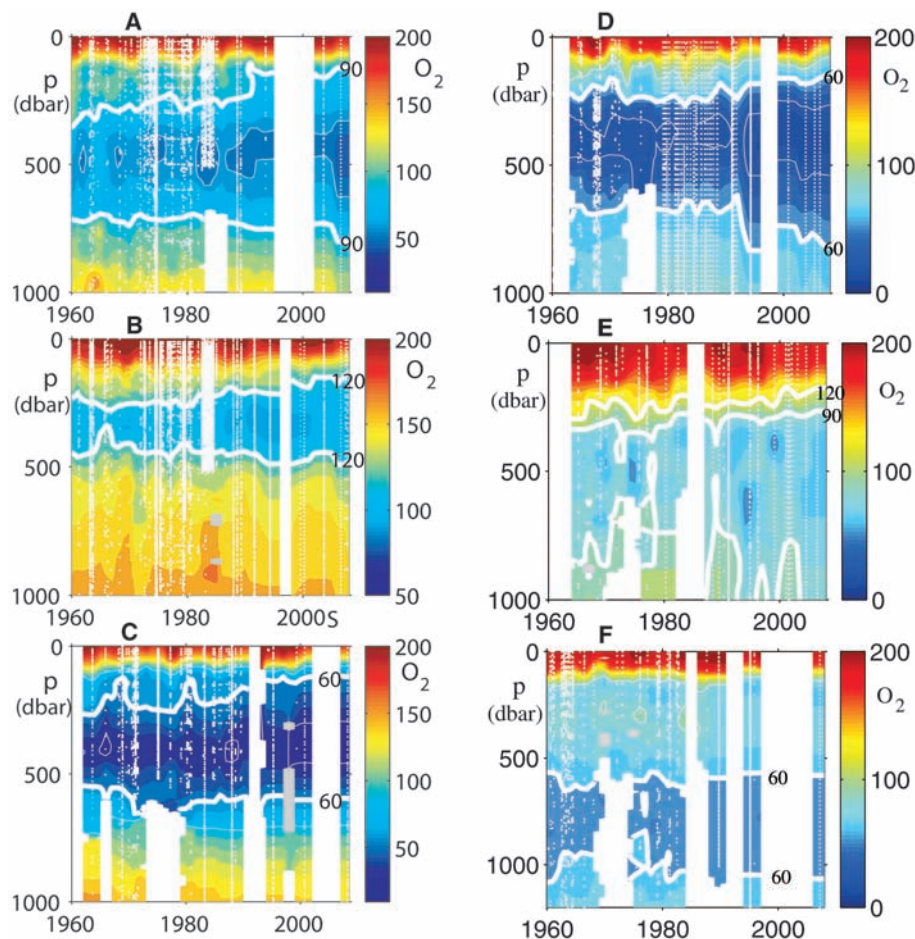


Fig. 2. Dissolved oxygen concentration ($\mu\text{mol kg}^{-1}$ shown in color maps (20, 21) versus time (1960–2008) and pressure (1 dbar ~ 1 m) with sample locations (white dots). (A) The eastern tropical North Atlantic (10° to 14°N , 20° to 30°W), contoured at $90 \mu\text{mol kg}^{-1}$ (thick white line). (B) The central equatorial Atlantic (3°S to 3°N , 28° to 18°W), contoured at $120 \mu\text{mol kg}^{-1}$ (thick white line). (C) The eastern tropical South Atlantic at (14° to 8°S , 4° to 12°E), contoured at $60 \mu\text{mol kg}^{-1}$ (thick white line). (D) The eastern equatorial Pacific Ocean (5°S to 5°N , 105° to 115°W), contoured at $60 \mu\text{mol kg}^{-1}$ (thick white line). (E) The central equatorial Pacific Ocean (5°S to 5°N , 165° to 175°W), contoured at 90 and $120 \mu\text{mol kg}^{-1}$ (thick white lines). (F) The eastern equatorial Indian Ocean (5°S to 0 , 90° to 98°E), contoured at $60 \mu\text{mol kg}^{-1}$ (thick white line).

Table 1. Linear trends of temperature and oxygen with 95% confidence intervals (22) since 1960 in a 300- to 700-m layer for select ocean areas, and integrated oxygen loss, assuming a nominal density of 1027.2 kg m^{-3} .

Ocean areas (Fig. 1)	Temperature trend ($^{\circ}\text{C year}^{-1}$)	Oxygen trend ($\mu\text{mol kg}^{-1} \text{ year}^{-1}$)	Integrated oxygen loss ($\text{mmol m}^2 \text{ year}^{-1}$)
Area A	$+0.009 \pm 0.008$	-0.34 ± 0.13	136
Area B	$+0.005 \pm 0.008$	-0.19 ± 0.12	74
Area C	$+0.002 \pm 0.011$	-0.17 ± 0.11	74
Area D	-0.001 ± 0.009	-0.13 ± 0.32	49
Area E	-0.010 ± 0.008	-0.19 ± 0.20	74
Area F	$+0.005 \pm 0.007$	-0.09 ± 0.21	37
N. Pacific, 100 to 400 m depth (11)	$+0.005$ to $+0.012$	-0.39 to -0.70	165

References and Notes

- H. W. Bange, S. W. Naqvi, L. A. Codispoti, *Prog. Oceanogr.* **65**, 145 (2005).
- F. Joos *et al.*, *Eos* **84**, 197 (2003).
- J. S. Gray, R. S. Wu, Y. Y. Or, *Mar. Ecol. Prog. Ser.* **238**, 249 (2002).
- C. E. Jones, H. C. Jenkins, *Am. J. Sci.* **301**, 112 (2001).
- M. J. Benton, R. J. Twitchett, *Trends Ecol. Evol.* **18**, 358 (2003).
- P. B. Wignall, R. J. Twitchett, *Science* **272**, 1155 (1996).
- R. J. Matear, A. C. Hirst, *Global Biogeochem. Cycles* **17**, 10.1029/2002GB001997 (2003).
- L. Bopp, C. Le Quere, M. Heimann, A. C. Manning, P. Monfray, *Global Biogeochem. Cycles* **16**, 10.1029/2001GB001445 (2002).
- S. Levitus, J. I. Antonov, T. P. Boyer, C. Stephens, *Science* **287**, 2225 (2000).
- H. E. Garcia, T. P. Boyer, S. Levitus, R. A. Locarnini, J. Antonov, *Geophys. Res. Lett.* **32**, 10.1029/2004GL022286 (2005).
- F. A. Whitney, H. J. Freeland, M. Robert, *Prog. Oceanogr.* **75**, 179 (2007).
- R. J. Matear, A. C. Hirst, B. I. McNeil, *Geochem. Geophys. Geosyst.* **1**, 10.1029/2000GC000086 (2000).
- R. Curry, www.who.edu/science/PO/hydrobase/ (2007).
- W. J. Gould, J. Turton, *Weather* **61**, 17 (2006).
- A. Körtzinger, J. Schimanski, U. Send, D. R. W. Wallace, *Science* **306**, 1337 (2004).
- L. Stramma *et al.*, *J. Geophys. Res.* **113**, C04014, 10.29/2007J004369 (2008).
- L. Stramma, J. Fischer, P. Brandt, F. Schott, in *Interhemispheric Water Exchange in the Atlantic Ocean*, G. J. Goni, P. Malanotte-Rizzoli, Eds. (Elsevier, Amsterdam, 2003), pp. 1–22.

Downloaded from www.sciencemag.org on May 2, 2008

18. H. E. Garcia, R. A. Locarnini, T. P. Boyer, J. I. Antonov, in *World Ocean Atlas 2005, Vol. 3: Dissolved Oxygen, Apparent Oxygen Utilization, and Oxygen Saturation*, S. Levitus, Ed. (National Oceanic and Atmospheric Administration Atlas National Environmental Satellite, Data, and Information Service 63, U.S. Government Printing Office, Washington, DC, 2006), p. 1–342.
 19. R. Schlitzer, <http://odv.awi.de> (2007).
 20. HydroBase (13) quality-controlled data augmented with recent repeat transects and available Argo float profiles within the areas shown (Fig. 1) were objectively mapped using correlation scales of 1 year and 50 m. To ameliorate potential spatial bias due to recent sparser sampling, the meridional conductivity temperature depth and bottle sections used after 2000 were longitudinally centered within each area. Inspection of data distributions

suggests that reported trends are not based on geographical shifts of data locations inside the investigation areas or seasonal shifts as a function of time, except as noted in the text.
 21. Suspect data for 1989 were removed from Fig. 2D (offset from the surface to 1000 m), for 1963 from Fig. 2E (stations only in the southern part of the box), and for 1986 from Fig. 2F (oxygen increased from 400 m to a maximum at 1000 m).
 22. Linear trends and their 95% confidence intervals were estimated as in (23), using annual 300- to 700-m averages of the objectively mapped fields. Degrees of freedom for the confidence intervals were determined from integral time scales as in (24).
 23. C. Wunsch, *The Ocean Circulation Inverse Problem* (Cambridge Univ. Press, Cambridge, 1996).

24. H. von Storch, F. W. Zwiers, *Statistical Analysis in Climate Research* (Cambridge Univ. Press, Cambridge, 1999).
 25. The Deutsche Forschungsgemeinschaft provided support as part of the German project Sonderforschungsbereich 754 (L.S.). Additional support was provided through the National Oceanic and Atmospheric Administration (NOAA) Office of Oceanic and Atmospheric Research (G.C.J.) and NSF award no. 0223869 (J.S.). Findings and conclusions in this article are those of the authors and do not necessarily represent the views of NOAA. Float data are collected and made freely available by the international Argo Project and contributing national programs (www.argo.ucsd.edu).

6 December 2007; accepted 20 March 2008
 10.1126/science.1153847

A General Model for Food Web Structure

Stefano Allesina,^{1,2*} David Alonso,^{1,3} Mercedes Pascual^{1,4}

A central problem in ecology is determining the processes that shape the complex networks known as food webs formed by species and their feeding relationships. The topology of these networks is a major determinant of ecosystems' dynamics and is ultimately responsible for their responses to human impacts. Several simple models have been proposed for the intricate food webs observed in nature. We show that the three main models proposed so far fail to fully replicate the empirical data, and we develop a likelihood-based approach for the direct comparison of alternative models based on the full structure of the network. Results drive a new model that is able to generate all the empirical data sets and to do so with the highest likelihood.

Food webs (1–3) are paradigmatic examples of complex systems in nature (4). Despite the challenge posed by the intricacy of these trophic networks, simple models have been proposed for their topology that successfully capture a number of structural properties (5–7). These models have been influential in showing that the topology of food webs in nature is non-random and have provided a basis for investigating the consequences of their structure for dynamics (8, 6, 9), for an ecosystem's robustness to extinctions (10), and for the quantity and quality of services they provide (11, 12).

The simplest mathematical framework for food web structure dates back to the influential argument on stability and complexity, and it relied on the representation of connections between species based on random graphs (13). This model took into account only the species richness S and connectance C (fraction of realized feeding connections) of the web. The first nonrandom representation was given by the cascade model (5), which ordered species along a single dimension.

The biological basis for this ordering remains an open problem, but possibilities include body mass, trophic level, and metabolic rates (14, 9). Each species has a position in this hierarchy that determines its feeding relations, with prey chosen randomly only from the species whose ranking is lower than that of the predator. This rule makes all networks generated by this model acyclic, limiting its application to empirical food webs without cannibalism or feeding cycles. The niche model was proposed next (6, 15), in part to overcome this limitation. It retains the ordering of species in one dimension but adds the notion of a niche range, an interval that contains all the prey of a given predator. Although feeding cycles can now be generated, the resulting networks are, by construction, also interval, a property that is not

fully compatible with patterns in empirical food webs (7, 16).

Intervality has played an important role in the literature of food web models, because it is closely related to the number of dimensions needed to represent niches in a community (17, 7, 16). Technically, this property means that there exists a suitable ordering of the species for which all the prey of each predator are consecutive, with no gaps. In Fig. 1, matrix N , this property is apparent when the network is translated into a matrix representation; consecutive prey form an uninterrupted sequence of entries in each column. Although, for interval graphs, a single dimension should be sufficient, recent analyses indicate that food webs are only close to interval (16). As we show here, close to interval does not mean that a model assuming perfect intervality on a single axis can generate all the links in empirical food webs. A third and more recent model, the “nested hierarchy” (7), does not rely on niches in a one-dimensional space, but focuses instead on groups of species and considers implicitly phylogenetic constraints and adaptation (7). Closely related predators tend to share their prey with occasional departures from this phylogenetic constraint, as the result of adaptation to new environments and new prey (7). We focus here on these three static models of food web structure as the simplest and most used formulations; other models have been proposed that include more sophisticated construction rules, including dynamics and diet optimization, speciation, extinction, evolution (18–20), and adaptation (21).

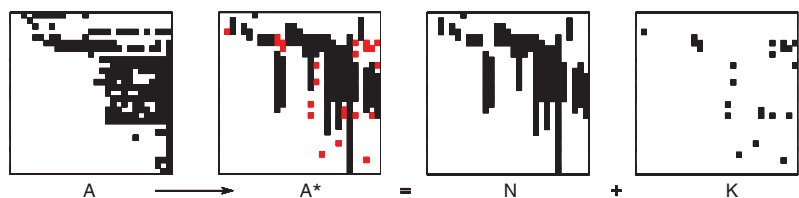


Fig. 1. Decomposition of a food web into two subwebs. For a given food web, we can write an adjacency matrix A . In this matrix, each coefficient represents the presence (1, black) or lack (0, white) of interaction between predator species (columns) and prey species (rows). We seek an ordering of the species that minimizes the number of irreducible connections, the links that are incompatible with the assumptions of a given model, in this case, the niche model. This yields the adjacency matrix A^* . The compatible connections of each predator i do fall into a segment (intervality) such that the segment starts either before or on the i th species (hierarchy). The matrix N is formed by all the connections compatible with the niche model, and the matrix K contains all the irreducible connections.

¹Department of Ecology and Evolutionary Biology, University of Michigan, Natural Science Building, 830 North University, Ann Arbor, MI 48109, USA. ²National Center for Ecological Analysis and Synthesis, 735 State Street, Suite 300, Santa Barbara, CA 93101, USA. ³Community and Conservation Ecology Group, Center for Ecological and Evolutionary Studies, University of Groningen, Post Office Box 14, 9750 AA Haren, Netherlands. ⁴Santa Fe Institute, 1399 Hyde Park Road, Santa Fe, NM 87501, USA.

*To whom correspondence should be addressed. E-mail: allesina@nceas.ucsb.edu